Philosophical Magazine Letters

Phase-field model for ferromagnetic shape-memory alloys

J. X. Zhang [a]; L. Q. Chen [a]
[a] Department of Materials Science and Engineering, The Pennsylvania State University. University Park, PA 16802. USA

PLEASE SCROLL DOWN FOR ARTICLE

Taylor & Francis
Taylor & Francis Group

Phase-field model for ferromagnetic shape-memory alloys

J. X. ZHANG* and L. Q. CHEN

Department of Materials Science and Engineering, The Pennsylvania State University,
University Park, PA 16802, USA

A computational model is developed to predict the ferroelastic and ferro-magnetic domain structures in ferromagnetic shape-memory alloys by combining the phase-field approach, micromagnetics and the microelasticity theory of Khachaturyan [*Theory of Structural Transformations in Solid* (Wiley, New York, 1983)]. As an example, the NiMnGa ferromagnetic shape-memory alloy is considered. Both the magnetic domain structures and martensite microstructures are studied. The emphasis is on the overall strain response and associated evolution of both magnetic domain structure and martensite microstructure under an applied magnetic field with different initial conditions. The results are compared with existing experiment measurements and observations.

1. Introduction

Ferromagnetic shape-memory alloys (FSMAs) are a relatively new class of active materials that generate very large strains in an applied magnetic field, more than an order of magnitude larger than those of conventional magnetostrictive materials [1–3]. The physical nature of FSMAs has been extensively studied experimentally [4–12]. Different characteristics of magnetization curves, i.e. square-like curves with a very high slope, roundish curves with low slopes and curves with discontinuities in their slopes, have been observed [1, 4–9]. These different behaviours are attributed to the various mechanisms of magnetization that depend on the microstructure and experimental conditions, including 180° magnetic domain-wall motion, magnetization rotation, twin-boundary motion and a combination of these.

Recently, several models have been proposed to understand the unique magneto-mechanical behaviour of the FSMAs [13–17]. The model proposed by James and Wuttig [13] is based on the minimization of external field, anisotropy, magnetostatic and elastic energies, while the exchange energy and strain gradient energy were not considered in the model. O'Handley [14] gave a two-dimensional analytical model analysing a two-variant system with a mobile twin boundary. Likhachev and Ullakko [15] have taken a more general thermodynamic approach. They integrated the Maxwell relation between the magnetic and stress–strain parameters to obtain the field-dependent strain. Thermodynamic models have been developed by Vasil'ev *et al.* [16] and L'vov *et al.* [17] to study the phase diagram of FSMAs describing

*Corresponding author. Email: jzz108@psu.edu

possible structural and magnetic transitions and the magnetization *versus* temperature behaviour. However, there has been essentially no direct prediction and simulation of simultaneous martensitic and magnetic domain structures and their evolution under external fields for FSMAs.

During the last decade, micromagnetic modeling has been used extensively to study the stability of magnetic domain structure and the magnetization process in magnetic materials [18, 19]. On the other hand, the phase-field model has been successfully applied to the prediction of martensite microstructure evolution in bulk [20–23] and thin-film [24] systems.

The main purpose of this letter is to describe a computational approach to modelling the stability of both martensite microstructures and magnetic domain structures and their sequential or simultaneous temporal evolution in FSMAs. It combines the phase-field model for proper martensitic transformations and the micromagnetic model for magnetic domain structure evolution. Such an approach considers all the energy contributions to martensite microstructure and magnetic domain structure. It is able to predict the detailed domain structure and martensite microstructure as well as their evolution under an applied field without *a priori* assumptions on domain and martensite plate morphologies. The results predicted from our simulations are compared with existing experimental observations.

2. Model description

In this approach, a given microstructure state is described by two fields: a local magnetization field, $M(r)$, and a stress-free transformation strain field, $\varepsilon_{ij}^o(r)$. While the magnetization field describes the magnetic domain structure, the stress-free strain field specifies the martensite microstructure.

The total free energy of an inhomogeneous ferromagnetic shape-memory alloy is given by

$$E = E_{\text{anis}} + E_{\text{exch}} + E_{\text{ms}} + E_{\text{external}} + E_{\text{Landau}} + E_{\text{gradient}} + E_{\text{me}} + E_{\text{elastic}}, \qquad (1)$$

where E_{anis}, E_{exch}, E_{ms}, E_{external}, E_{Landau}, E_{gradient}, E_{me}, and E_{elastic} are the magneto-crystalline anisotropy, magnetic exchange, magnetostatic, external field, Landau, strain gradient, magnetoelastic and elastic energies, respectively.

The magnetocrystalline anisotropy energy of a cubic crystal is

$$E_{\text{anis}} = \int \left[K_1 \left(m_1^2 m_2^2 + m_1^2 m_3^2 + m_2^2 m_3^2 \right) + K_2 m_1^2 m_2^2 m_3^2 \right] dV, \qquad (2)$$

where m_i are the components of the unit magnetization vector, $\boldsymbol{m} = \boldsymbol{M}/M_s$, M_s is the saturation magnetization, K_1 and K_2 are the anisotropy constants.

The exchange energy is determined solely by the spatial variation of the magnetization orientation and can be written as

$$E_{\text{exch}} = A \int (\text{grad}\,\mathbf{m})^2 dV, \qquad (3)$$

where A is the exchange stiffness constant.

The magnetostatic energy of a system can be written as

$$E_{ms} = -\frac{1}{2}\mu_0 M_s \int \boldsymbol{H}_d \cdot \boldsymbol{m} \, dV, \tag{4}$$

where $\boldsymbol{H}_d$ is the demagnetization field that is determined by the long-range interactions among the magnetic moments in the system, and μ_0 is the permeability of vacuum.

We separate the local magnetization field into a sum of a spatially independent average magnetization and a spatially dependent heterogeneous part, i.e. $\boldsymbol{M}(\mathbf{r}) = \overline{\boldsymbol{M}} + \delta\boldsymbol{M}(\mathbf{r})$. The average field $\overline{\boldsymbol{M}}$ is defined in such a way that $\int \delta\boldsymbol{M}(\mathbf{r})dV = 0$. The magnetic field $\boldsymbol{H}_d$ due to the heterogeneous magnetization $\delta\boldsymbol{M}(\mathbf{r})$ is calculated by solving the Maxwell's equation div $\boldsymbol{B} = \text{div}(\mu_0\boldsymbol{H} + \mu_0\boldsymbol{M}) = 0$, while the demagnetization field caused by the average magnetization is approximated by $\boldsymbol{H}_d(\overline{\boldsymbol{M}}) = N\overline{\boldsymbol{M}}$, where N is the demagnetizing factor, which depends only on the shape of a specimen. Such an approach is an approximation for incorporating the effect of sample shape on domain structures, which is, in principle, only valid if the simulation system size is much smaller than the real sample size to be simulated. The calculation of the magnetostatic energy is described in detail in [25].

The effect of an external applied magnetic field $\boldsymbol{H}_{ex}$ on the system energy can be taken into account through the interaction between the magnetization and the external field, or so-called the Zeeman energy,

$$E_{external} = -\mu_0 M_s \int \boldsymbol{H}_{ex} \cdot \boldsymbol{m} \, dV. \tag{5}$$

The Landau free energy describing the proper martensitic transformation is given by [16, 26, 27]

$$E_{Landau} = \int \left[Q_1 e_1^2 + Q_2\left(e_2^2 + e_3^2\right) + Q_3 e_3\left(e_3^2 - 3e_2^2\right) + Q_4\left(e_2^2 + e_3^2\right)^2 + Q_5\left(e_4^2 + e_5^2 + e_6^2\right) \right] dV \tag{6}$$

where Q_1, Q_2, and Q_5 are bulk, deviatoric and shear modulus, respectively. Q_3 and Q_4 denote third- and fourth-order elastic constants. e_i are the symmetry-adapted strain defined in term of the transformation strains as [16]:

$$e_1 = \left(\varepsilon_{11}^0 + \varepsilon_{22}^0 + \varepsilon_{33}^0\right)/\sqrt{3}, \qquad e_4 = \varepsilon_{23}^0,$$

$$e_2 = \left(\varepsilon_{11}^0 - \varepsilon_{22}^0\right)/\sqrt{2}, \qquad\qquad e_5 = \varepsilon_{13}^0, \tag{7}$$

$$e_3 = \left(2\varepsilon_{33}^0 - \varepsilon_{22}^0 - \varepsilon_{11}^0\right)/\sqrt{6}, \qquad e_6 = \varepsilon_{12}^0,$$

Since a cubic to tetragonal martensitic transition was studied here, we set $\varepsilon_{23}^0 = \varepsilon_{13}^0 = \varepsilon_{12}^0 = 0$ in this letter for simplicity. The Landau free-energy describes a first-order cubic to tetragonal transition where the austenite phase (cubic) is described by $(\varepsilon_{11}^0 = 0, \varepsilon_{22}^0 = 0, \varepsilon_{33}^0 = 0)$ and the martensite phase is described by $\text{tet}_1 = (-\varepsilon_0, 1/2\varepsilon_0, 1/2\varepsilon_0)$, $\text{tet}_2 = (1/2\varepsilon_0, -\varepsilon_0, 1/2\varepsilon_0)$ and $\text{tet}_3 = (1/2\varepsilon_0, 1/2\varepsilon_0, -\varepsilon_0)$ corresponding to the three tetragonal variants, where ε_0 is the magnitude of the

spontaneous strain at a given temperature. Such a strain-based formalism has been used by Saxena and co-workers [28, 29] to study the evolution of microstructure in ferroelastic materials.

The energy contribution of a wall between two tetragonal variants (twin boundary) is introduced through gradients of the order parameters

$$E_{\text{gradient}} = \int \left\{ \frac{1}{2} g \left[\left(\varepsilon^0_{11,1} \right)^2 + \left(\varepsilon^0_{11,2} \right)^2 + \left(\varepsilon^0_{11,3} \right)^2 + \left(\varepsilon^0_{22,1} \right)^2 \right.\right.$$
$$\left.\left. + \left(\varepsilon^0_{22,2} \right)^2 + \left(\varepsilon^0_{22,3} \right)^2 + \left(\varepsilon^0_{33,1} \right)^2 + \left(\varepsilon^0_{33,2} \right)^2 + \left(\varepsilon^0_{33,3} \right)^2 \right] \right\} dV \qquad (8)$$

where g is the strain gradient coefficient. In this letter, a comma in a subscript stands for spatial differentiation, for example, $\varepsilon^0_{ii,j} = \partial \varepsilon^0_{ii} / \partial x_j$, where x_j is the jth component of position vector in the Cartesian coordinates.

For a cubic system, the magnetoelastic energy is given by

$$E_{\text{me}} = \int \left\{ B \left[\varepsilon^0_{11} \left(m_1^2 - \frac{1}{3} \right) + \varepsilon^0_{22} \left(m_2^2 - \frac{1}{3} \right) + \varepsilon^0_{33} \left(m_3^2 - \frac{1}{3} \right) \right] \right\} dV \qquad (9)$$

where B is the magnetoelastic coefficient, which is a measure of degree of coupling between strain and magnetization.

If we assume that the interfaces developed during microstructure evolution are coherent, elastic strains e_{ij} and thus elastic energy E_{elastic} are generated,

$$e_{ij} = \varepsilon_{ij} - \varepsilon^0_{ij}, \qquad (10)$$

where ε_{ij} is the total strain. The corresponding elastic energy can be expressed as

$$E_{\text{elastic}} = \int \frac{1}{2} c_{ijkl} e_{ij} e_{kl} \, dV = \int \frac{1}{2} c_{ijkl} \left(\varepsilon_{ij} - \varepsilon^0_{ij} \right) \left(\varepsilon_{kl} - \varepsilon^0_{kl} \right) dV, \qquad (11)$$

where c_{ijkl} is the second-order elastic stiffness tensor. The summation convention for the repeated indices is employed and $i, j, k, l = 1, 2, 3$. The elastic energy and elastic interactions are obtained using the microelasticity theory of Khachaturyan [30].

The temporal evolution of the magnetization configuration, thus the domain structure, is described by the Landau–Lifshitz–Gilbert (LLG) equation

$$\left(1 + \alpha^2 \right) \frac{\partial \boldsymbol{M}}{\partial t} = -\gamma_0 \boldsymbol{M} \times \boldsymbol{H}_{\text{eff}} - \frac{\gamma_0 \alpha}{M_{\text{s}}} \boldsymbol{M} \times \left(\boldsymbol{M} \times \boldsymbol{H}_{\text{eff}} \right), \qquad (12)$$

where γ_0 is the gyromagnetic ratio, α is the damping constant, and $\boldsymbol{H}_{\text{eff}}$ is the effective magnetic field

$$\boldsymbol{H}_{\text{eff}} = -\frac{1}{\mu_0} \frac{\partial E}{\partial \boldsymbol{M}}. \qquad (13)$$

The temporal martensitic microstructure evolution is described by the time-dependent Ginzburg–Landau (TDGL) equations

$$\frac{\partial \varepsilon^0_{ii}(x, t)}{\partial t} = -L \frac{\delta E}{\delta \varepsilon^0_{ii}} \qquad (14)$$

where L is the kinetic coefficient.

3. Results and discussion

We use the NiMnGa alloy as an example for our numerical simulations. We solved the LLG equation employing the Gauss–Seidle projection method [31] and TDGL equation using the semi-implicit Fourier-spectral method [32]. The following materials parameters are used [5, 33]: $M_s = 6.02 \times 10^5$ A/m, $K_1 = 2.7 \times 10^3$ J/m^3, and $K_2 = -6.1 \times 10^3$ J/m^3, $A = 2 \times 10^{-11}$ J/m. The coefficients in the Landau free-energy and the magnetoelastic coefficient were obtained by fitting the experimental measurements [5, 34], i.e. $Q_1 = 2.32 \times 10^{11}$ J/m^3, $Q_{20} = 3.78 \times 10^8$ J/m^3 ($Q_2 = Q_{20}(T - T_M)/T_M$), $Q_3 = 0.40 \times 10^{10}$ J/m^3, $Q_4 = 7.50 \times 10^{10}$ J/m^3 and $B = 4.00 \times 10^6$ J/m^3. The martensitic transformation temperature is $T_m = 300$ K, and the simulation temperature is chosen to be $T = 250$ K. For a bulk tetragonal NiMnGa crystal, the elastic constants are $c_{11} = 1.70 \times 10^{11}$ N/m^2, $c_{33} = 1.50 \times 10^{11}$ N/m^2, $c_{12} = 1.50 \times 10^{11}$ N/m^2, $c_{13} = 1.54 \times 10^{11}$ N/m^2, $c_{44} = 0.40 \times 10^{11}$ N/m^2, $c_{66} = 0.45 \times 10^{11}$ N/m^2 [35]. To avoid solving an elastic equation with inhomogeneous modulus, we choose c_{11} as the average of c_{11} and c_{33}, c_{12} the average of c_{12} and c_{13}, and c_{44} the average of c_{44} and c_{66}, i.e. $c_{11} = 1.60 \times 10^{11}$ N/m^2, $c_{12} = 1.52 \times 10^{11}$ N/m^2 and $c_{44} = 0.43 \times 10^{11}$ N/m^2. To save the computational time, we performed the simulations with $256 \times 256 \times 1$ discrete cells, i.e. essentially two-dimensional systems. Periodic boundary conditions are applied along the x_1, x_2, and x_3 axes. The time step for integration is $\Delta t/t_0 = 0.1$, where $t_0 = ((1 + \alpha^2)/\gamma_0 M_s)$. The cell size is 18 nm; thus, the system size studied here is around $4.6 \times 4.6\,\mu$m. We also did simulations with a cell size of 9 nm and obtained similar results.
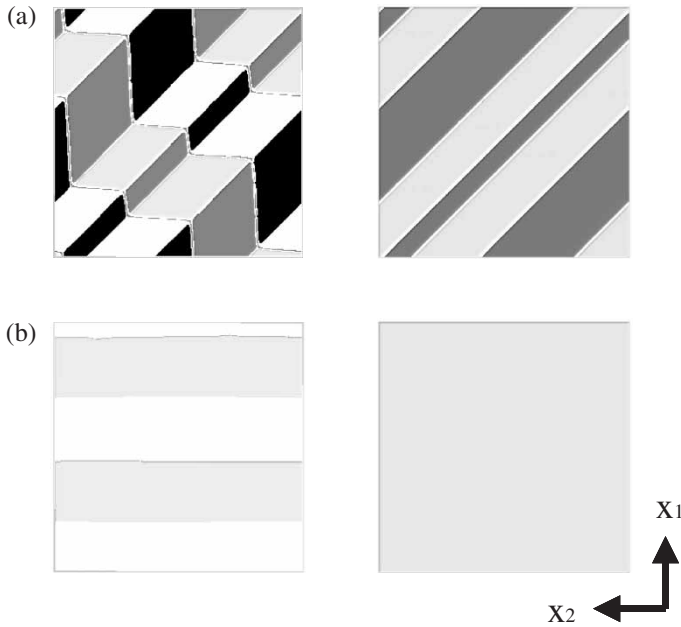
Figure 1. Simulated magnetic domain structures (left side: black = $\boldsymbol{m}$ // [$\bar{1}$00], dark gray = $\boldsymbol{m}$ // [100], white = $\boldsymbol{m}$ // [0$\bar{1}$0], light gray = $\boldsymbol{m}$ // [010]) and martensite microstructures (right side: dark gray = tet$_1$, light gray = tet$_2$) of FSMAs. (a) Without applied stress, (b) with applied tensile stress along x_1.

Figure 1a shows a simulated microstructure with both magnetic domains and martensites. The initial condition was created by assigning random orientation for the magnetization field and a zero value plus a small random noise for the martensite strain order parameters. Two kinds of martensitic variants were observed, and the twin boundary is along the $[1\bar{1}0]$ direction, which is determined by the condition of elastic compatibility. Staircase-like magnetic domain structure was observed, with magnetization vectors orienting along the easy axis associated with the martensite variants. The 90° domain walls coincide with the twin boundaries, indicating coupling between magnetic domains and martensitic twins. Each martensitic plate contains anti-parallel magnetic domains separated by 180° domain walls, which is favored by the minimization of the magnetostatic energy. The obtained magnetic domain structure agrees well with the experiment observation of two-variant specimen [10]. Figure 1b shows the morphologies of magnetic domains and martensites under an applied tensile stress along x_1 axis, where a single martensite variant was obtained. The simulations predicted correctly the experimentally observed stripe magnetic domain structure [10]. The direction of the 180° domain walls was parallel to the magnetization vectors, which is consistent with the magnetic compatibility condition. It should be pointed out that our current simulations are performed in 2D; it is desirable to extend the work to 3D since in this case there are three tetragonal martensite variants in the system and as a result more complicated domain structures can develop. The requirement of magnetic compatibility and elastic compatibility for the three tetragonal martensite variants will result in a multilevel hierarchy in the domain structure [36]. Corresponding 3D work is under way.

The magnetization process of the twin structure obtained in figure 1a under an applied magnetic field (along x_1 axis) was studied. In figure 2, there is a discontinuity in the slope of the M/M_s vs. applied field curve around 160 kA/m, and such a change also happens in plot of strain *versus* applied field. Those simulated results agree well with prior experimental measurements [4, 5]. The magnetic domain structures and martensitic microstructures shown in figure 3 clearly reveal that such discontinuous behaviours are due to different mechanisms of magnetization. While 180° domain wall motion occurred with no change of martensitic microstructure in the initial stage, in the later stage, the martensite twin boundaries began to move and, thus, the 90° magnetic domain wall movement.
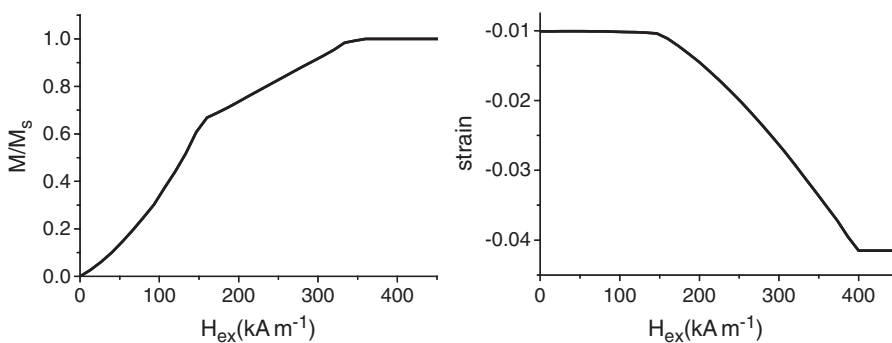
Figure 2. M/M_s vs. applied field and strain vs. applied field curves for the sample obtained in figure 1a.
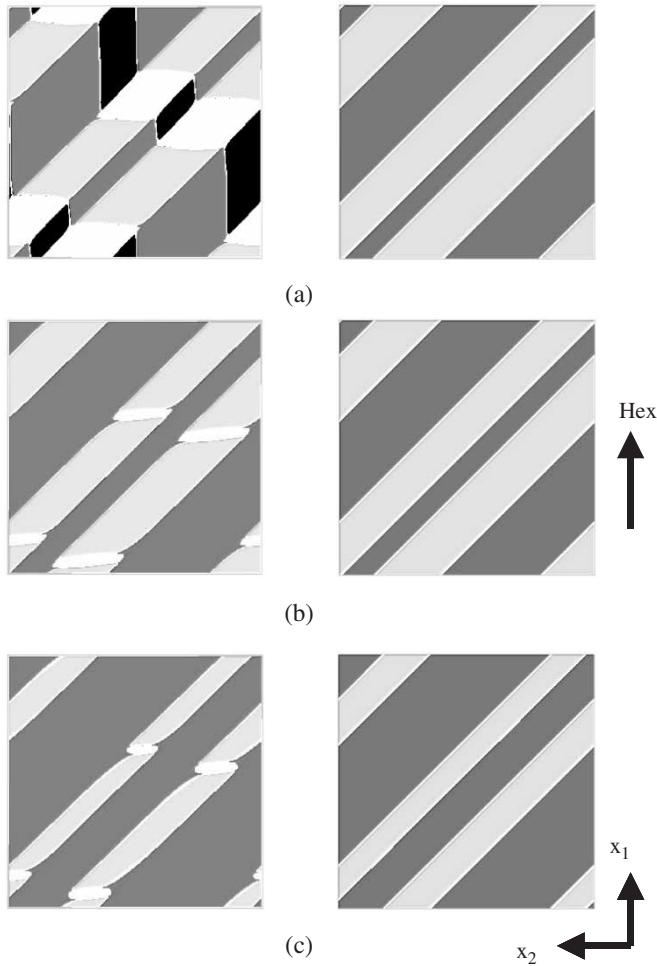
Figure 3. Evolution of magnetic domain structure (left side) and martensite microstructure (right side) under an applied magnetic field for the sample obtained in figure 1a. (a) 95 kA/m, (b) 175 kA/m, (c) 265 kA/m.

The magnetization process of a single-variant martensite obtained in figure 1b was also studied. Different magnetization curves were obtained as shown in figure 4. The 180° domain wall motion occurs when the applied field is along the easy axis of the martensite (x_2), while rotation of magnetization is responsible for the magnetization behaviour when the applied field is perpendicular to the easy axis. Since the heterogeneous nucleation of new martensite variant was not considered in our current model, no strain change was observed in both cases. The simulation results obtained in this case agree well with the experiment observation when the nucleation and growth of the second variant were prevented by experimental conditions, such as applied stress [5, 8]. Figure 4 shows M/M_s and strain *vs.* applied field curves for a single-variant martensite with the existence of a small residual second martensite variant. A sudden increase of the slope occurs in M/M_s *vs.* applied
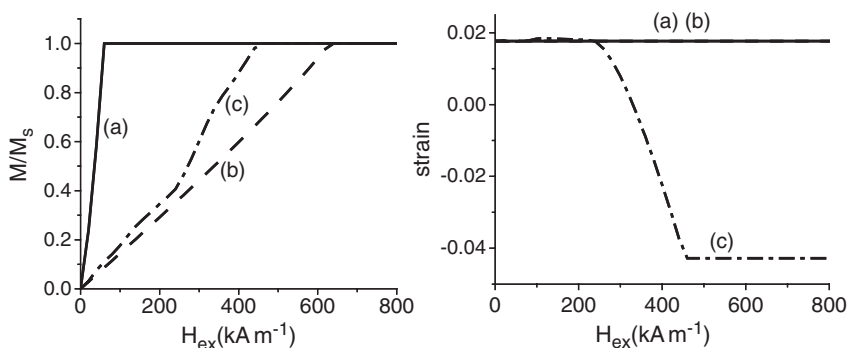
Figure 4. M/M_s *vs.* applied field and strain *vs.* applied field curves for the single-variant (tet$_2$) martensite sample. (a) $\boldsymbol{H}_{ex} \,/\!/ \, x_2$, (b) $\boldsymbol{H}_{ex} \perp x_2$, (c) $\boldsymbol{H}_{ex} \perp x_2$ (with the existence of residual second martensite variant).

field curve, and the strain *vs.* applied field curve given in figure 4 shows that such a slope change is associated with a strain change. The discontinuous behaviour observed here is due to the growth of the residual second martensite variant. Similar magnetization behaviours have been investigated experimentally [6–8], which confirmed the important effect of the second martensite variant on the magnetization behaviour of a single-variant martensite sample.

4. Summary

In summary, we have developed a computational model to predict the micro-structures of ferromagnetic shape-memory alloys and their temporal evolution by combining the phase-field approach, micromagnetics and the microelasticity theory of Khachaturyan [30]. The stability of martensite microstructure and magnetic domain structure of NiMnGa alloys were studied and the results agree well with prior experiment observations. The strain and associated domain structure evolution under an applied field were also simulated. Different M/M_s and strain *vs.* applied field curves were obtained, revealing the various magnetization mechanisms for NiMnGa alloys.

Acknowledgements

References

[1] K. Ullakko, J.K. Huang, C. Kantner, *et al.*, Appl. Phys. Lett. **69** 1966 (1996).
[2] R.C. O'Handley, S.J. Murray, M. Marioni, *et al.*, J. Appl. Phys. **87** 4712 (2000).

[3] T. Kakeshita and K. Ullakko, MRS Bull. **Feb.** 105 (2002).
[4] G.H. Wu, C.H. Yu, L.Q. Meng, *et al*., Appl. Phys. Lett. **75** 2990 (1999).
[5] R. Tickle and R.D. James, J. Magn. Magn. Mater. **195** 627 (1999).
[6] O. Heczko, A. Sozinov and K. Ullakko, IEEE Trans. Magn. **36** 3266 (2000).
[7] O. Heczko, K. Jurek and K. Ullakko, J. Magn. Magn. Mater. **226/230** 996 (2001).
[8] O. Heczko, L. Straka and K. Ullakko, J. Phys. IV Paris **112** 959 (2003).
[9] N. Okamoto, T. Fukuda, T. Kakeshita, *et al*., Sci. Technol. Adv. Mater. **5** 29 (2004).
[10] Y. Ge, O. Heczko, O. Soderberg, *et al*., J. Appl. Phys. **96** 2159 (2004).
[11] K. Koho, J. Vimpari, L. Straka, *et al*., J. Phys. IV Paris **112** 943 (2003).
[12] A. Sozinov, A.A. Likhachev, N. Lanska, *et al*., J. Phys. IV Paris **115** 121 (2004).
[13] R.D. James and M. Wuttig, Phil. Mag. A **77** 1273 (1998).
[14] R.C. O'Handley, J. Appl. Phys. **83** 3263 (1998).
[15] A.A. Likhachev and K. Ullakko, Phys. Lett. A **275** 142 (2000).
[16] A.N. Vasil'ev, A.D. Bozhko, V.V. Khovailo, *et al*., Phys. Rev. B **59** 1113 (1999).
[17] V.A. L'vov, E.V. Gomonaj and V.A. Chernenko, J. Phys.: Condens. Matter. **10** 4587 (1998).
[18] J. Fidler and T. Schrefl, J. Phys. D: Appl. Phys. **33** R135 (2000).
[19] J. Fidler, R.W. Chantrell, T. Schrefl, *et al*., in *Encyclopedia of Materials: Science and Technology*, edited by K.H.J. Buschow, R.W. Cahn, M.C. Flemings, *et al*. (Elsevier, Amsterdam, 2001).
[20] Y. Wang and A.G. Khachaturyan, Acta Mater. **45** 759 (1997).
[21] A. Artemev, Y. Wang and A.G. Khachaturyan, Acta Mater. **48** 2503 (2000).
[22] A. Artemev, Y. Jin and A.G. Khachaturyan, Acta Mater. **49** 1165 (2001).
[23] Y.M. Jin, A. Artemev and A.G. Khachaturyan, Acta Mater. **49** 2309 (2001).
[24] D.J. Seol, S.Y. Hu, Y.L. Li, *et al*., Mater. Sci. Forum **408/412** 1645 (2002).
[25] J.X. Zhang and L.Q. Chen, Acta Mater. **53** 2845 (2005).
[26] A.E. Jacos, S.H. Curnoe and R.C. Desai, Phys. Rev. B **68** 224104 (2003).
[27] J.K. Liakos and G.A. Saunders, Phil. Mag. A **46** 217 (1982).
[28] A. Saxena, T. Lookman, A.R. Bishop, *et al*., J. Phys. IV Paris **112** 85 (2003).
[29] K. Rasmussen, T. Lookman, A. Saxena, *et al*., Phys. Rev. Lett. **87** 055704 (2001).
[30] A.G. Khachaturyan, in *Theory of Structural Transfomations in Solid* (Wiley, New York, 1983).
[31] X.P. Wang and C.J. Garcia-Cervera, J. Comp. Phys. **171** 357 (2001).
[32] L.Q. Chen and J. Shen, Comput. Phys. Commun. **108** 147 (1998).
[33] D.I. Paul, J. Marquiss and D. Quattrochi, J. Appl. Phys. **93** 4561 (2003).
[34] N. Glavatska, G. Mogilniy, I. Glavatsky, *et al*., J. Phys. IV Paris **112** 963 (2003).
[35] L. Dai, J. Cullen and J. Cui, *et al*., Mater. Res. Soc. Symp. Proc. **785** D 2.2 (2004).
[36] A. Kazaryan, Y. Wang, Y.M. Jin, *et al*., J. Appl. Phys. **92** 7408 (2002).